Ab initio theoretical study of luminescence properties of Pr^{3+}-doped Lu_2O_3

José Luis Pascual,[1] Zoila Barandiarán,[2,3] and Luis Seijo[2,3,*]

[1]*Departamento de Química Física Aplicada, Universidad Autónoma de Madrid, 28049 Madrid, Spain*

[2]*Departamento de Química, Universidad Autónoma de Madrid, 28049 Madrid, Spain*

[3]*Instituto Universitario de Ciencia de Materiales Nicolás Cabrera, Universidad Autónoma de Madrid, 28049 Madrid, Spain*

(Dated: January 11, 2011)

Abstract

Ab initio embedded cluster calculations have been performed on Pr^{3+}-doped Lu_2O_3, in order to investigate the mechanism responsible for the highly efficient $^3P_0 \rightarrow {}^1D_2$ non-radiative relaxation experimentally observed. $(PrO_6)^{9-}$ embedded clusters representing the C_2 and S_6 substitutional sites of Pr^{3+}:Lu_2O_3 have been studied using wave function based methods. It is found that an outwards relaxation of the first coordination sphere around the impurity takes place upon doping. At the relaxed geometry of the lowest spin triplet $4f5d$ state, all the $4f5d$ states lie much higher in energy than all $4f^2$ states (except the ^{1}S multiplet). This result is in opposition to the interpretation of intersystem crossing through a low-lying $4f5d$ excited state of Pr^{3+} as the mechanism for the fast non-radiative $^3P_0 \rightarrow {}^1D_2$ relaxation proposed in the literature. Absorption to the lowest spin triplet $4f5d$ state is calculated to be around 4800 cm^{-1} higher for the C_2 site than for the S_6 site, supporting the assignment of bands in the excitation spectrum previously reported.

I. INTRODUCTION

Pr^{3+}-doped ionic solids are a useful class of phosphors. The electronic structure of the ion can give rise to luminescence in the ultraviolet (UV), visible and infrared (IR) wavelength ranges. Some Pr^{3+}-doped fluorides have been investigated as promising candidates for luminescence lamps due to the fact that they exhibit photon cascade emission[1]. Praseodymium-doped oxides have been considered as potentials lasers in the visible and IR domains[2].

Another important application is as phosphors in fast decay scintillators for X-ray computed tomography. For example, Gd_2O_2S:Pr has been used to that end.[3,4] The predominant radiative transitions of Pr^{3+} (ground electronic configuration $4f^2$) upon X-ray excitation occur from the $^3P_0$ and $^1D_2$ excited levels, to the $^3H_4$ ground level. The $^3P_0 \rightarrow {}^3H_4$ transition exhibits a very short decay time (in the μs scale) while the $^1D_2 \rightarrow {}^3H_4$ transition is slower (decay time in the ms scale).[5,6] As decay times much faster than the response times of the detector systems are required for scintillators,[3] phosphors which exhibit transitions only from the $^3P_0$ are preferred for X-ray computed tomography. $^3P_0 \rightarrow {}^1D_2$ non-radiative transitions are key factors in the suitability of the materials as fast decay scintillators. Knowledge of the mechanisms of non-radiative transitions is important for the proper design of this kind of materials.

Following this line, experimental studies have been performed to gain a better understanding of these mechanisms in Pr^{3+}-doped solids. Pr^{3+}-doped rare earth sesquioxides, especially yttrium sesquioxide, form a family of compounds that have been studied in relation to their luminescence properties.[2,5–8] Depending on the crystal symmetry and substitution site, Pr^{3+}-doped rare earth sesquioxides are found to emit preferentially from the $^3P_0$ state (hexagonal phases, monoclinic phases with high coordination) or from the $^1D_2$ state (monoclinic phases with low coordination, cubic phases).[8]

DeMello Donegá *et al.*[6] have studied the mechanisms that contribute to Pr^{3+} $^3P_0 \rightarrow {}^1D_2$ non-radiative relaxation in a large number of oxide hosts, including lutetium sesquioxide (Lu_2O_3). Several mechanisms are taken into account in their study:[6] (i) Multiphonon relaxation; (ii) cross-relaxation within pairs of Pr^{3+} ions; (iii) intersystem crossing through a low-lying $4f5d$ excited state of Pr^{3+}; (iv) intersystem crossing through a low-lying Pr-to-metal charge transfer state. A fifth mechanism, relaxation through Pr^{3+}-trapped exciton states, has been invoked to explain the quenching of the $^3P_0$ luminescence in Pr^{3+}-doped

$LiNbO_3$,[9] and the different behaviour of Pr^{3+}-doped $LiNbO_3$ and $LiTaO_3$.[10] Intersystem crossing through Pr-to-metal charge transfer states, sometimes referred to as *virtual recharge* mechanism, has been extensively invoked to explain the luminescent properties of a number of Pr-doped hosts containing complex oxoanions, such as titanates, vanadates and niobates (eg. see Refs. 11,12 and references therein).

The spectral properties of Pr^{3+}-doped Lu_2O_3 were experimentally investigated by DeMello Donegá *et al.*[6]. They recorded excitation and emission spectra and, from them, they obtained estimations of the radiative and non-radiative decay constants. They observed that cubic Lu_2O_3:Pr^{3+}emits only from the $^1D_2$ state. The fact that lowest $4f5d$ excited states lie around 36,000 cm^{-1}, that is, relatively low in energy, suggested that the dominant mechanism for the very highly efficient $^3P_0 \rightarrow {}^1D_2$ non-radiative relaxation could be intersystem crossing through the $4f5d$ excited states of Pr^{3+}.[6] In order to account for the different experimental observations, the authors tentatively proposed a configurational coordinate diagram (Fig. 7 in Ref. 6) for the system. The main features of this diagram were that the force constant of the $4f5d$ excited state is much greater than that of the $4f^2$ states and that the energy of the relaxed $4f5d$ excited state lies between the $^3P_0$ and $^1D_2$ levels ($4f^2$). A shortening of the Pr-O distances upon doping is invoked to explain these facts. The validity of these hypothesis can be checked in *ab initio* quantum mechanical calculations, which is one of the objectives of this work.

In this paper, we present theoretical *ab initio* calculations on the electronic structure of Pr^{3+}-doped Lu_2O_3. We have performed spin-free *ab initio* model potential (AIMP) embedded cluster optimizations of the geometry in relevant electronic states and then, we have calculated vertical transition energies at the optimal geometries. The AIMP embedded cluster method[13,14] has been succesfully applied in a number of structural and spectroscopical studies of lanthanide and actinide-doped ionic hosts.[15–20] As a result of the calculations, we obtain the local distortion produced by the Pr^{3+} doping and we give support to the assignments of the absorption bands to Pr^{3+} occupying different sites in the Lu_2O_3 lattice[5,6] are supported. The energy minima of the lowest $4f5d$ states are calculated and located with respect to the $4f^2$ $^3P_0$ and $^1D_2$ levels and possible luminescence after $4f \rightarrow 5d$ excitation is predicted. In spite of the computational demands required by the theoretical results presented here, this paper is only a first step into the elucidation of the electronic structure of the Pr^{3+} defect in cubic rare earth sesquioxides. Further calculations on more compli-

cated mechanisms such as the *virtual recharge* mechanism and intersystem crossing through Pr^{3+}-trapped exciton states are underway in our laboratory.

The paper is organized as follows: in Sec. II we briefly describe the method used together with the details of the calculations. The results of the calculations are presented in Sec. III and a discussion of them is presented in Sec. IV. We present the conclusions in Sec. V.

II. METHOD

A. Structure of the Lu_2O_3 host

The crystal structure of Lu_2O_3 is of the rare earth sesquioxide C-type structure, the bixbyite structure, cubic with space group $Ia\bar{3}(T_h^7)^{21}$ (see Fig. 1). The lattice parameter of Lu_2O_3 is a_0=10.931 Å. In the bixbyite structure there are two crystallographically different cations sites. In Lu_2O_3, 24 Lu^{3+} cations occupy the Wyckoff position 24d at (u, 0, 1/4) and 8 Lu^{3+} cations occupy the Wyckoff position 8b at (1/4, 1/4, 1/4). The oxygen atoms occupy the general 48e position at (x, y, z). The coordination polyhedra are distorted cubes, in which six corners are occupied by oxygen ionsand the remaining two are vacant. The resulting coordination polyhedra around both cations are depicted in Fig. 2. In the case of the Lu^{3+} 24d ions, the vacant sites are located along a face diagonal of the cube, leading to site symmetry C_2. In the case of the Lu^{3+} 8b ions, the two oxygens are missing along the body diagonal of the cube, and the resulting site symmetry is S_6 (or C_{3i}). The internal parameters of Lu_2O_3 have not been experimentally determined to our knowledge. Instead, they have been obtained by periodic density-functional theory calculations using the generalized-gradient approximation, as reported in Ref. 22. The resulting internal parameters are: u=-0.0330, x=0.3912, y=0.1521, z=0.3800. In the C_2 site there are three pairs of neighboring oxygen ions at three different distances, in the S_6 site all six oxygen ions are at the same distance. These perfect lattice data are summarized in Table I.

The ratio of C_2 to S_6 sites in 3:1. It is believed that, when an impurity substitutes for a lattice cation in cubic sesquioxides, it enters both crystallographic sites[5] and spectral features have been interpreted in the literature[5,6] assuming this, as commented below. Stanek *et al.* have studied the site preference of trivalent dopant ions in bixbyite sesquioxides[23], by atomic-scale simulations using classic pair potentials, and they have found a marked preference for

S_6 site substitution in Pr^{3+}:Lu_2O_3. In this work we have studied both substitutional sites.

B. Details of the calculations

The local geometries around the Pr^{3+} ion and the transition energies reported in this work have been calculated using embedded cluster wave function based methods. For this purpose, $(PrO_6)^{9-}$ clusters were embedded in *ab initio* model potential (AIMP)[13,14] representations of the pure Lu_2O_3 host. The clusters chosen to model the C_2 and S_6 sites are shown on Fig. 2. AIMP total ion embedding potentials, calculated in this work, were located at the perfect Lu_2O_3 ionic positions. They accurately reproduce the quantum-mechanical interactions between the external crystal ions (Lu^{3+} and O^{2-} ions) and the wavefunctions associated with the point defect $(PrO_6)^{9-}$ clusters. They include electrostatic (Coulomb and short range corrections), exchange and Pauli repulsion interactions and they have been produced using the recipes of Refs. 13 and 14. Embedding AIMPs were used at all lattice ions located within a cube of length $3a_0$ centered at the impurity site. The remaining ions within a cubic shell of length $5a_0$ are treated as point charges and Evjen's method[24] is used to define the charge of the frontier ions.

Bonding, static and dynamic correlation, and scalar relativistic effects within the $(PrO_6)^{9-}$ clusters have been taken into account by performing state averaged complete active space self-consistent field (SA-CASSCF)[25] and multistate second order perturbation theory (MS-CASPT2)[26–28] calculations using a scalar relativistic many-electron Hamiltonian. The relativistic effective [Kr]-core model potential and $(14s10p10d8f3g)/[6s5p6d4f1g]$ Gaussian valence basis set, taken from Refs. 29 and 30 were used for Pr. The [He]-core effective core potential and $(5s6p1d)/[3s4p1d]$ Gaussian valence basis set, taken from Ref. 31, were used for oxygen, extended with one p-type diffuse function for anion[32] and one d-type polarization function.[33] Spin-orbit coupling has not been included in the calculations; thus, comparison with experimental data are semiquantitative. As we show below, inclusion of spin-orbit effects should not alter the conclusions of this work. These calculations were performed using the program MOLCAS.[34] All the model potentials (core and embedding) and basis sets used in this work are available from the authors.[35]

In a first step, the geometry of the clusters was optimized at the CASSCF level. The CAS space was chosen so that it comprises all configurations in which two electrons occupy

the thirteen molecular orbitals of main character Pr $4f$, Pr $5d$ and Pr $6s$. In the case of the S_6 site, we performed the calculations using C_i symmetry. The molecular orbitals were chosen so as to minimize the average energy of all states with dominant $4f^2$ (21 ^3A_g states, 28 ^1A_g states) or $4f5d$ and $4f6s$ configurational character (42 ^3A_u states, 42 ^1A_u states). The cluster geometry was optimized for the 1 ^3E_g state (lowest spin triplet $4f^2$ state) and the 1 ^3A_u state (lowest spin triplet $4f5d$ state). The resulting optimized geometries were very nearly S_6 symmetric.

In the case of the C_2 site, we performed the calculations without any symmetry (point group C_1). The molecular orbitals were chosen so as to minimize the average energy of all states with dominant $4f^2$, $4f5d$ and $4f6s$ configurational character (63 ^3A states, 63 ^1A states). The cluster geometry was optimized for the 1 ^3B state (lowest spin triplet $4f^2$ state) and the 13 ^3B state (lowest spin triplet $4f5d$ state). The resulting optimized geometries were very nearly C_2 symmetric.

We have calculated the vertical transition energies at the CASSCF $4f^2$ and $4f5d$ optimized geometries using the MS-CASPT2 method. A total of 58 electrons, which occupy the orbitals with main character Pr $5s$, $5p$, $4f$, $5d$ and $6s$ (10 electrons) and O $2s$, $2p$ (48 electrons), have been correlated. An imaginary shift[36] of 0.10 au. has been used in the calculations to ensure that no intruder states are present. Large and uniform weights of the reference wavefunctions (around 70 %) were found in the CASPT2 calculations. We will refer to these calculations as MS-CASPT2(O48,Pr10).

III. RESULTS

A. Local distortions

We present the optimized Pr-O distances for the lowest $4f^2$ and $4f5d$ spin triplet states both at the C_2 and S_6 sites in Table I together with the geometry of the perfect Lu_2O_3 lattice calculated at Ref. 22. First, it can be seen that, upon doping, the Pr-O distances are larger than in the perfect lattice, for both sites. This result is totally in line with previous calculations performed in similar systems: the results upon doping qualitatively reflect the mismatch of ionic radii between the dopant ion and the substituted host ion and are quantitatively smaller. In this case, the radii are 0.86 Å for Lu^{3+} and 0.99 Å for Pr^{3+}

(both in coordination number 6).[37]

The Pr-O distances shorten by about 0.01 Å at the C_2 site and by about 0.02 Å at the S_6 site upon $4f \rightarrow 5d$ excitation. In the case of the C_2 site, the different Pr-O distances behave differently: two of them (Pr-O(1) and Pr-O(5)) shorten while the third one (Pr-O(3)) remains esentially unchanged. This shortening is in agreement with what has been found in other lanthanides and actinides in high symmetry halide coordination[15,16,18,20,38], and recently has been experimentally concluded.[39] An extensive study of the factors leading to this result for several ions, including Pr^{3+}, can be found in Ref. 40. Recent results on Ce^{3+}-doped YAG[17] show that this shortening upon excitation is also found in the case of lower symmetry sites. Our results for Pr^{3+}-doped Lu_2O_3 are in line with these latter results.

The calculation of the optimized geometries do not include spin-orbit nor electron correlation effects. The effect of the lack of spin-orbit in the structures should be negligible, in the line of what we have found in similar systems.[16,18] The only exception are those systems and states in which spin-orbit coupling mixes states belonging to different dominant electron configurations.[20] This is not the case here, as the separation between the relevant $4f^2$ and $4f5d$ manifolds is large (see below).

The effect of the inclusion of electron corrrelation in the geometry optimization should be a uniform shortening of less than 0.02 Å in the equilibrium distances.[41] This additional shortening does not change the main conclusion of this section, viz. the outwards distortion of the clusters caused by doping in the Pr^{3+}:Lu_2O_3 lattice.

B. Relative energies of the $4f^2$ and $4f5d$ manifolds

Table II presents vertical transition energies of the $(PrO_6)^{9-}$ embedded clusters, with respect to the $4f^2$ ground state, at different cluster geometries, for the C_2 site and the S_6 site. For each cluster, we have calculated the vertical transition energies at the $4f^2$ ground state equilibrium geometry and at the optimal geometry of the lowest spin triplet $4f5d$ state. Vertical transition energies have also been calculated at the geometry of the perfect Lu_2O_3 lattice for the C_2 site. All the transition energies have been computed at the MS-CASPT2(O48,Pr10) level. The data in the Table are also shown in Fig. 3. The electronic states are grouped according to their main $4f^2$, $4f5d$ or $4f6s$ configurational chareacter. Such a disticnction is done by inspection of the wavefunctions and symmetry

(g/u) considerations.

The $4f^2$ manifold spans 25 000 cm^{-1} in both sites, the only exception being the state related to the $4f^2$-^{1}S multiplet, which lies at much higher energy and is inmersed in the $4f5d$ electronic manifold. It can be seen that the vertical transition energies to the ^{3}F, ^{1}G, and ^{1}I multiplets are very similar for both sites, but the rest of the multiplets lie at lower energies in the C_2 site than in the S_6 site: 1100 cm^{-1} for ^{1}D, 3300 cm^{-1} for ^{3}P, and 4700 cm^{-1} for ^{1}S.

The $4f5d$ manifold, both for the C_2 and S_6 sites, appear to be well above the $4f^2$ states. The $4f^2$-$4f5d$ energy gap is 13 500 cm^{-1} in the C_2 site and 9300 cm^{-1} in the S_6 site. Relaxation of the geometry of the lowest spin triplet $4f5d$ states does not modify this picture. Relaxation energies are 450 cm^{-1} and 1050 cm^{-1} for the C_2 and S_6 sites, respectively.

The $4f5d$ manifolds show different submanifold structure in the two sites due, basically, to the different crystal field splitting of the excited $5d$ electron. The centroids of the $4f5d$ levels are at 52 670 cm^{-1} (C_2) and 52 600 cm^{-1} (S_6), and the difference between the lowest level and the centroids are 15 005 cm^{-1} (C_2) and 18 740 cm^{-1} (S_6). These data suggest that the ligand field effects are larger in the S_6 site.

The vertical transition energies presented in Table II do not include indirect effects of dynamic correlation through the optimized geometries, since the optimization has been done at the CASSCF level. As commented above, a systematic bond length shortening should be expected as a consequence of dynamic correlation effects.[41] An estimation of such indirect effect can be deduced by comparing the the transition energies evaluated at the perfect lattice geometry and at the $4f^2$ ground state relaxed geometry for the C_2 site, since the bond lengths are shorter in the former structure. This comparison allows to conclude that the indirect effect of dynamic corrrelation are not significant and, more important for the objective of this work, do not alter the energy gaps between the $4f^2$ and $4f5d$ manifolds.

Spin-orbit coupling is also absent in the calculations of the vertical transition energies. Yet, previous calculations on a very similar system like Ce^{3+}-doped YAG[17] show that spin-orbit effects decrease the $4f$-$5d$ energy gap by less than 550 cm^{-1}. Thus, spin-orbit coupling cannot be expected to reduce the calculated $4f^2$-$4f5d$ energy gap so as to locate the lowest $4f5d$ states within the $4f^2$ manifold.

IV. DISCUSSION

We discuss here the local distortion produced by the Pr^{3+} impurity, the possibility of intersystem crossing through $4f5d$ excited states, and some observed spectral features of Pr^{3+}-doped Lu_2O_3 using the results of Section III.

We focus first on the distortion of the Lu_2O_3 lattice due to the Pr^{3+} impurity. An inwards distortion due to strong Pr-O orbital mixing has been suggested,[6] in order to account for the spectral features of the material. The present calculations lead to an outwards distortion of the first coordination sphere which is smaller than suggested by the mismatch of ionic radii due to strong metal-ligand mixing.

This inwards distortion was invoked in relation to the extremely fast Pr^{3+} $^3P_0 \rightarrow {}^1D_2$ non-radiative relaxation found in the material. This relaxation has been suggested to be due to intersystem crossing through low-lying $4f5d$ states. A configurational coordination diagram to account for the relaxation has been presented[6] where the $4f5d$ minimum energy lies below the $^3P_0$ level and above and close to the $^1D_2$ level, which would provide a path for $^3P_0 \rightarrow {}^1D_2$ non radiative relaxation. The present *ab initio* results show that the energy of the lowest $4f5d$ states is well above all the $4f^2$ (except the state related to ^{1}S-$4f^2$, as we commented above) even after excited state relaxation is considered and they do not support intersystem crossing through $4f5d$ states as the quenching mechanism. Other mechanisms should be investigated in order to explain the high non-radiative decay rate found in Ref. 6.

We will focus now on the different spectral features that have been reported in Ref. 6. As we commented above, the lack of spin-orbit effects in our calculations allows to make only semiquantitative comparisons with experimentally determined spectral features. This fact is more severe for f-f transitions than for f-d, as the former should be more influenced by spin-orbit coupling. The emission and excitation spectra of Pr^{3+}:Lu_2O_3 have been reported in Ref. 6. In the excitation spectra, several lines are reported between 16 600 and 17 540 cm^{-1}, assigned to excitations to the ^{1}D multiplet levels; another group of lines between 20 000 and 23 800 cm^{-1} is assigned to $^3H \rightarrow {}^3P$, ^1I transitions. The calculations show a good semiquantitative agreement with these data. The position of the $^3H_4 \rightarrow {}^3P_0$ zero-phonon line is reported to be 19 996 cm^{-1}; the present calculation for the lowest $^3H \rightarrow {}^3P$ transition in C_2 site (the most frequent site) is 19 220 cm^{-1}. The gap between the $^1D_2$ and the $^3P_0$ levels is reported to be 2600 cm^{-1} whereas we predict 2700 cm^{-1}; spin-orbit splitting of the

$^3P_0$-related levels is expected to lower the theoretical gap and to lead, perhaps, to a certain underestimation when spin-orbit coupling is considered. The crystal field splitting of the $^1D_2$ multiplet is found to be 1280 cm^{-1} and our data slightly overestimate it (1920 cm^{-1}, site C_2; 1800 cm^{-1}, site S_6); spin-orbit coupling is not expected to be important in this.

A broad band, with a maximum at 36 200 cm^{-1} and a shoulder at 30 300 cm^{-1} is reported in the excitation spectra. By comparison with other measurements on Pr^{3+}:Ln_2O_3 (Ln= Y, Sc, Gd),[5] they are ascribed to $4f^2 \rightarrow 4f5d$ transitions within Pr^{3+} ions at C_2 and S_6 sites in Lu_2O_3, respectively. This is in contrast with the conclusions of the pair-potential studies[23], that predict only S_6 substitution in this lattice. According to the present calculations, the lowest $4f^2 \rightarrow 4f5d$ (triplet states) excitation energies are 38 690 and 33 860 cm^{-1} for the C_2 and S_6 sites, respectively. Thus, the *ab initio* calculations support the assignment done in Ref. 6 of the higher energy band to the Pr^{3+} ions occupying the C_2 site and the shoulder to Pr^{3+} ions occupying the S_6 site.

Both for C_2 and S_6 sites, there is a large gap in energy between the highest level of the $4f^2$ manifold and the lowest level of the $4f5d$ manifold. At the lowest spin triplet $4f5d$ geometry, this gap amounts 12 900 cm^{-1} for the C_2 site and 8 000 cm^{-1} for the S_6 site. The highest lying ^{1}S multiplet is inmersed in the $4f5d$ manifold in both sites. The lowest spin-triplet $4f5d$ state should be metastable and emission from it should be expected under $4f5d$ excitation. However, no such emission is experimentally observed.[6] Instead, identical emission is found under $^3P_0$ excitation and under $4f5d$ excitation.[6] Thus, some mechanism should exist in the material for efficient non-radiative $4f5d \rightarrow {}^1D_2$ relaxation. This mechanism is likely to be the same that provides a fast $^3P_0 \rightarrow {}^1D_2$ relaxation.

V. CONCLUSIONS

We have performed *ab initio* model potential calculations of the electronic structure of $(PrO_6)^{9-}$ embedded clusters that represent the C_2 and S_6 sites of Pr^{3+}-doped lutetium sesquioxide. We have performed spin-free CASSCF optimizations of the geometry around the Pr^{3+} impurity and, at the equilibrium geometries of the $4f^2$ and $4f5d$ lowest spin triplet states, we have performed MS-CASPT2 calculations of the vertical transition energies from the ground state to all the states coming from the $4f^2$, $4f5d$ and $4f6d$ manifolds, both for spin triplet and singlet. As a result of the geometry optimization, we find an outwards distor-

tion of the first coordination shell around the impurity upon doping. The transition energy from the minimum of the lowest $4f5d$ state is found to be well above the position of both $^3P_0$ and $^1D_2$ levels, (around 10,000 cm^{-1}) strongly suggesting that intersystem crossing through this $4f5d$ state is not the dominant mechanism for $^3P_0 \rightarrow {}^1D_2$ non-radiative relaxation. The calculations also predict strong $4f5d \rightarrow 4f^2$ luminescence under $4f5d$ excitation. However, this luminescence is absent in the experimental results[6], suggesting that some mechanism is quenching it, probably the same mechanism responsible for the $^3P_0$ emission quenching. Other quenching mechanisms have to be investigated to explain the fast non-radiative relaxation. In this line, calculations in order to investigate the *virtual recharge* mechanism[11,12] and relaxation via intersystem crossing through trapped exciton states[9,10] are underway in our laboratory. Finally, the present calculations do support the interpretation of the $4f5d$ band maximum and shoulder found in the excitation spectrum[6] of Pr^{3+}-doped Lu_2O_3 as due to electronic transitions of Pr^{3+} ions located at C_2 and S_6 sites, respectively.

Acknowledgments

This work was partly supported by a grant from Ministerio de Ciencia e Innovación, Spain (Dirección General de Programas y Transferencia de Conocimiento MAT2008-05379/MAT).

---

* Corresponding author; Electronic address: luis.seijo@uam.es

[1] S. Kück, I. Sokólska, M. Henke, M. Döring, and T. Scheffler, J. Lumin. **102-103**, 176 (2003).

[2] Y. Guyot, R. Moncorgé, L. D. Merkle, A. Pinto, B. McIntosh, and H. Verdun, Opt. Mater. **5**, 127 (1996).

[3] H. Yamada, A. Suzuki, Y. Uchida, M. Yoshida, H. Yamamoto, and Y.Tsukuda, J. Electrochem. Soc. **136**, 2713 (1989).

[4] W. W. Moses, in *Inorganic Scintillators and Their Applications, SCINT99*, edited by V. V. Mikhailin (Moscow State University, Moscow, 2000), p. 11.

[5] G. C. Aumüller, W. Köstler, B. C. Grabmaier, and R. Frey, J. Phys. Chem. Solids **55**, 767 (1994).

[6] C. de Mello Donegá, A. Meijerink, and G. Blasse, J. Phys. Chem. Solids **56**, 673 (1995).

[7] M. Arai, N. Matsuda, and M. Tamatani, J. Alloys Comp. **192**, 45 (1993).

[8] M. Okumura, M. Tamatani, A. K. Albessard, and N. Matsuda, Jpn. J. Appl. Phys. **36**, 6411 (1997).

[9] C. Koepke, K. Wisniewski, D. Dyl, M. Grinberg, and M. Malinowski, Opt. Mater. **28**, 137 (2006).

[10] W. Gryk, C. Dujardin, M.-F. Joubert, W. Ryba-Romanowski, M. Malinowski, and M. Grinberg, J. Phys.: Condensed Matter **18**, 117 (2006).

[11] P. Boutinaud, R. Mahiou, E. Cavalli, and M. Betinelli, Chem. Phys. Lett. **418**, 185 (2006).

[12] P. Boutinaud, E. Pinal, M. Oubaha, R. Mahiou, E. Cavalli, and M. Betinelli, Opt. Mater. **28**, 9 (2006).

[13] Z. Barandiarán and L. Seijo, J. Chem. Phys. **89**, 5739 (1988).

[14] L.Seijo and Z. Barandiarán, in *Computational Chemistry: Reviews of Modern Trends - Vol. 4*, edited by J. Leszczynski (World Scientific, Singapore, 1999), p. 55.

[15] Z. Barandiarán and L. Seijo, J. Chem. Phys. **118**, 7439 (2003).

[16] B. Ordejón, M. Karbowiak, L. Seijo, and Z. Barandiarán, J. Chem. Phys. **125**, 074511 (2006).

[17] J. Gracia, L. Seijo, Z. Barandiarán, D. Curulla, H. Niemansverdriet, and W. van Gennip, J. Lumin. **128**, 1248 (2008).

[18] G. Sánchez-Sanz, L. Seijo, and Z. Barandiarán, J. Phys. Chem. A **113**, 12591 (2009).

[19] G. Sánchez-Sanz, L. Seijo, and Z. Barandiarán, J. Chem. Phys. **133**, 114506 (2010).

[20] G. Sánchez-Sanz, L. Seijo, and Z. Barandiarán, J. Chem. Phys. **133**, 114509 (2010).

[21] R. W. G. Wyckoff, *Crystal Structures* (Wiley, New York, 1963).

[22] L. Marsella and V.Fiorentini, Phys. Rev. B **69**, 172103 (2004).

[23] C. R. Stanke, K. J. McClellan, B. P. Uberuaga, K. E. Sickafus, M. R. Levy, and R. W. Grimes, Phys. Rev. B **75**, 134101 (2007).

[24] H. M. Evjen, Phys. Rev. **39**, 675 (1932).

[25] B. O. Roos, P. R. Taylor, and P. E. M. Siegbahn, Chem. Phys. **48**, 157 (1980); P. E. M. Siegbahn, A. Heiberg, J. Almlöf, and B. O. Roos, J. Chem. Phys. **74**, 2384 (1981); P. Siegbahn, A. Heiberg, B. Roos, and B. Levy, Phys. Scr. **21**, 323 (1980).

[26] K. Andersson, P.-Å. Malmqvist, B. O. Roos, A. J. Sadlej, and K. Wolinski, J. Phys. Chem. **94**, 5483 (1990); K. Andersson, P.-Å. Malmqvist, and B. O. Roos, J. Chem. Phys. **96**, 1218 (1992).

[27] A. Zaitsevskii and J. P. Malrieu, Chem. Phys. Lett. **233**, 597 (1995).

[28] J. Finley, P.-Å. Malmqvist, B. O. Roos and L. Serrano-Andrés, Chem. Phys. Lett. **288**, 299 (1998).

[29] L. Seijo, Z. Barandiarán, and E. Harguindey, J. Chem. Phys. **114**, 118 (2001).

[30] L. Seijo, Z. Barandiarán, and B. Ordejón, Mol. Phys. **101**, 73 (2003).

[31] S. Huzinaga, Z. Barandiarán, L. Seijo, and M. Klobukowsky, J. Chem. Phys. **86**, 2132 (1987).

[32] T. H. Dunning, Jr. and P. J. Hay, in *Modern Theoretical Chemistry*, edited by H. F. Schaeffer III (Plenum, New York, 1977).

[33] J. Andzelm, M. Klobukowsky, E. Radzio-Andzelm, Y. Sakai, and H. Tatewaki, *Gaussian Basis Sets for Molecular Calculations* (Elsevier, Amsterdam, 1984).

[34] G. Karlström, R. Lindh, P.-Å. Malmqvist, B. O. Roos, U. Ryde, V. Veryazov, P.-O. Widmark, M. Cossi, B. Schimmelpfennig, P. Neogrady, and L. Seijo, Comp. Mater. Sci. **28**, 222 (2003).

[35] Detailed core and embedding AIMP data libraries in electronic format are available from the authors upon request or directly at the address http://www.uam.es/quimica/aimp/Data/AIMPLibs.html. See also Ref. 34.

[36] N. Forsberg and P.-A. Malmqvist, Chem. Phys. Lett. **274**, 196 (1997).

[37] R. D. Shannon, Acta Cryst. **A32**, 751 (1976).

[38] F. Ruipérez, L. Seijo, and Z. Barandiarán, J. Chem. Phys. **122**, 234507 (2005).

[39] R. Valiente, F. Rodríguez, J. González, H. U. Güdel, R. Martín-Rodríguez, L. Nataf, M. N. Sanz-Ortiz, and K. Krämer, Chem. Phys. Lett. **481**, 149 (2009).

[40] Z. Barandiarán and L. Seijo, J. Chem. Phys. **119**, 3785 (2003).

[41] J. L. Pascual, N. Barros, Z. Barandiarán, and L. Seijo, J. Phys. Chem. A **113**, 12454 (2009).

TABLE I: Lu-O and Pr-O equilibrium distances for the C_2 and S_6 polyhedra in the Lu_2O_3 and Lu_2O_3:Pr^{3+} crystals, respectively. Lu-O distances have been taken from Ref. 22. Pr-O distances have been optimized for the lowest spin triplet $4f^2$ and $4f5d$ states at the CASSCF level in this work. Lattice distortions produced by the Pr^{3+} impurity in parenthesis. All distances in Å.

			Pr-O	
		Lu-O	$4f^2$	$4f5d$
C_2 site				
	O(1)	2.289	2.343 (0.054)	2.335
	O(3)	2.223	2.294 (0.071)	2.295
	O(5)	2.200	2.225 (0.025)	2.201
	O(avg.)	2.237	2.287 (0.050)	2.277
S_6 site				
	O	2.239	2.302 (0.063)	2.280
Mismatch of ionic radii			0.13[a]	

[a]Radii taken from Ref. 37

TABLE II: Vertical transition energies of the $(PrO_6)^{9-}$ embedded cluster calculated at the C_2 and S_6 sites. Transition energies calculated at the C_2 site using the perfect Lu_2O_3 lattice, relaxed $1\,^3B$-$4f^2$ and relaxed $13\,^3B$-$4f5d$ cluster geometries. Transition energies calculated at the S_6 site using the relaxed $1\,^3E_g$-$4f^2$ and relaxed $1\,^3A_u$-$4f5d$ cluster geometries. The calculations include 58 valence electron correlation, static relativistic effects and Lu_2O_3 embedding host effects. (MS-CASPT2(O48,Pr10) level) All numbers are in cm^{-1}.

	C_2 cluster geometry			S_6 cluster geometry		
	perfect lattice	relaxed $4f^2$	relaxed $4f5d$		relaxed $4f^2$	relaxed $4f5d$
$4f^2$ manifold						
from ^{3}H						
$1\,^3B$	0	0	0	$1\,^3E_g$	0	0
$2\,^3B$	100	275	180	$1\,^3A_g$	95	110
$1\,^3A$	150	280	325	$2\,^3E_g$	610	640
$2\,^3A$	630	745	750	$2\,^3A_g$	800	815
$3\,^3B$	810	895	915	$3\,^3A_g$	1130	1205
$3\,^3A$	840	960	1030	$3\,^3E_g$	1250	1325
$4\,^3A$	1255	1215	1215	$4\,^3E_g$	1980	2125
$4\,^3B$	1455	1467	1530			
$5\,^3B$	1730	1715	1755			
$5\,^3A$	1795	1830	1905			
$6\,^3B$	1865	1870	1900			
from ^{3}F						
$6\,^3A$	4385	4390	4410	$4\,^3A_g$	4800	4845
$7\,^3B$	4810	4775	4815	$5\,^3E_g$	5325	5440
$8\,^3B$	4920	5015	5125	$5\,^3A_g$	5355	5405
$9\,^3B$	5095	5185	5235	$6\,^3E_g$	5780	5925
$7\,^3A$	5195	5190	5180	$6\,^3A_g$	6075	6205
$8\,^3A$	5365	5330	5350			
$10\,^3B$	5690	5590	5640			
from ^{1}G						
$1\,^1B$	5645	5835	5825	$1\,^1E_g$	5540	5530
$1\,^1A$	5715	5560	5615	$1\,^1A_g$	5655	5685
$2\,^1B$	5805	6013	6005	$2\,^1A_g$	5895	5910
$2\,^1A$	5905	6045	6075	$2\,^1E_g$	6095	6110
$3\,^1B$	6380	6495	6505	$3\,^1E_g$	7065	7155
$3\,^1A$	6760	6300	6330	$3\,^1A_g$	7645	7750
$4\,^1A$	7035	7170	7225			
$5\,^1A$	7560	7495	7560			
$4\,^1B$	7760	7675	7735			
from ^{1}D						
$6\,^1A$	14400	14595	14525	$4\,^1E_g$	15685	15650
$7\,^1A$	14910	15255	15300	$4\,^1A_g$	16357	16410
$5\,^1B$	15395	15475	15520	$5\,^1E_g$	17480	17555
$6\,^1B$	16315	16385	16390			
$8\,^1A$	16520	16515	16550			
from ^{3}P						
$11\,^3B$	18985	19220	19280	$7\,^3E_g$	22665	22675
$12\,^3B$	20875	21220	21335	$7\,^3A_g$	23840	23985
$9\,^3A$	21395	21435	21365			
from ^{1}I						
$9\,^1A$	20285	20760	20700	$5\,^1A_g$	21070	20985

TABLE II: (continued)

	perfect lattice	relaxed $4f^2$	relaxed $4f5d$		relaxed $4f^2$	relaxed $4f5d$
$7\ ^1B$	20735	21035	21100	$6\ ^1A_g$	21530	21485
$10\ ^1A$	20865	21150	21150	$6\ ^1E_g$	21575	21505
$8\ ^1B$	20945	21375	21300	$7\ ^1E_g$	21650	21575
$11\ ^1A$	21540	21540	21660	$7\ ^1A_g$	22125	22155
$9\ ^1B$	21730	21970	22190	$8\ ^1E_g$	23430	23495
$12\ ^1A$	22295	22305	22105	$9\ ^1E_g$	24375	24545
$10\ ^1B$	22355	22430	22380	$8\ ^1A_g$	24515	24780
$11\ ^1B$	22395	22550	22670	$9\ ^1A_g$	24560	24850
$13\ ^1A$	22735	22650	22595			
$14\ ^1A$	23180	23090	22985			
$15\ ^1A$	24955	25125	25280			
$12\ ^1B$	25065	25205	25340			
from ^{1}S						
$19\ ^1A$	40840	41680	41690	$10\ ^1A_g$	46345	46365
$4f^15d^1$ manifold (up to 50 000 cm^{-1})						
spin triplet states						
$13\ ^3B$	38105	38690	38250	$1\ ^3A_u$	33860	32800
$10\ ^3A$	38375	39220	38740	$2\ ^3A_u$	34680	33690
$11\ ^3A$	38980	40125	39485	$1\ ^3E_u$	34720	33740
$14\ ^3B$	39840	39840	39530	$2\ ^3E_u$	36505	35540
$15\ ^3B$	39895	40280	39840	$3\ ^3A_u$	36550	35790
$16\ ^3B$	40130	40690	40970	$3\ ^3E_u$	37795	37490
$17\ ^3B$	40400	41275	41405	$4\ ^3A_u$	38405	38235
$12\ ^3A$	40590	41420	41330	$4\ ^3E_u$	38905	38725
$13\ ^3A$	40975	41935	41560	$5\ ^3A_u$	39100	38850
$18\ ^3B$	41210	41665	41830	$5\ ^3E_u$	40480	40280
$14\ ^3A$	41260	42130	41910	$6\ ^3A_u$	41205	40950
$19\ ^3B$	41515	42200	42570	$7\ ^3A_u$	41280	41090
$15\ ^3A$	41790	42390	42395	$6\ ^3E_u$	41640	41420
$16\ ^3A$	42395	43535	43565	$7\ ^3E_u$	42950	42950
$20\ ^3B$	42710	43335	43340			
$21\ ^3B$	42800	43680	43795			
$22\ ^3B$	43930	44700	44940			
$17\ ^3A$	44085	44615	44265			
$18\ ^3A$	44475	45080	44925			
$23\ ^3B$	44755	45150	45030			
$19\ ^3A$	44860	45700	45940			
spin singlet states						
$16\ ^1A$	37235	37815	37405	$1\ ^1A_u$	33770	33120
$13\ ^1B$	37630	38070	37560	$1\ ^1E_u$	34665	33900
$14\ ^1B$	38460	38975	38590	$2\ ^1A_u$	35340	34490
$17\ ^1A$	39550	40030	39560	$2\ ^1E_u$	35715	34965
$18\ ^1A$	39655	40200	39830	$3\ ^1E_u$	37870	37570
$15\ ^1B$	40340	41170	40930	$3\ ^1A_u$	38555	38115
$16\ ^1B$	41640	42055	41330	$4\ ^1A_u$	39360	38540
$20\ ^1A$	41770	42355	42170	$4\ ^1E_u$	42040	41690
$21\ ^1A$	41930	42550	42355	$5\ ^1A_u$	42440	42300
$17\ ^1B$	42370	43220	42490	$5\ ^1E_u$	42590	42360
$18\ ^1B$	42485	43530	43850	$6\ ^1A_u$	42775	42510
$22\ ^1A$	43510	44220	44005	$6\ ^1E_u$	43260	43010
$23\ ^1A$	43740	44315	44290	$7\ ^1A_u$	46480	46220
$19\ ^1B$	43755	44355	44280	$7\ ^1E_u$	46965	46720
$20\ ^1B$	44405	45075	45055			
$24\ ^1A$	44500	45230	45085			
$25\ ^1A$	45240	46395	46430			
$21\ ^1B$	45385	46455	46400			

TABLE II: (continued)

	perfect lattice	relaxed $4f^2$	relaxed $4f5d$		relaxed $4f^2$	relaxed $4f5d$
22 ^1B	47105	48100	48160			
26 ^1A	47850	48900	49055			
23 ^1B	48450	48860	48850			
$4f^15d^1$ + $4f^16s^1$ manifold						
spin triplet states						
20-22^3A, 24-27^3B	58355-60950	58810-61225	57820-60350	8-11^3A_u, 8-12^3E_u	71670-76230	72215-76925
23-29^3A, 28-34^3B	75025-79610	75770-79965	76775-80750	12-14^3A_u, 13-14^3E_u	82330-85830	80650-84370
spin singlet states						
27-29^1A, 24-27^1B	59170-63300	59410-63570	58430-62745	8-11^1A_u, 8-12^1E_u	71085-82100	71695-80240
30-36^3A, 28-34^1B	74005-83880	75580-85520	76075-85460	12-14^1A_u, 13-14^1E_u	82880-86405	81755-84925

Figure captions

FIG. 1: Cubic cell of the bixbyite structure showing the C_2 and S_6 coordination polyhedra around the dopant ion.

FIG. 2: Schematic representation of the C_2 and S_6 coordination polyhedra around the cations in the bixbyite structure.

FIG. 3: Energy levels of Pr^{+3}:Lu_2O_3 as calculated in this work. Energy levels are calculated at the relaxed $4f^2$ and $4f5d$ geometries, both for C_2 and S_6 sites. All numbers are calculated at the MS-CASPT2 level.

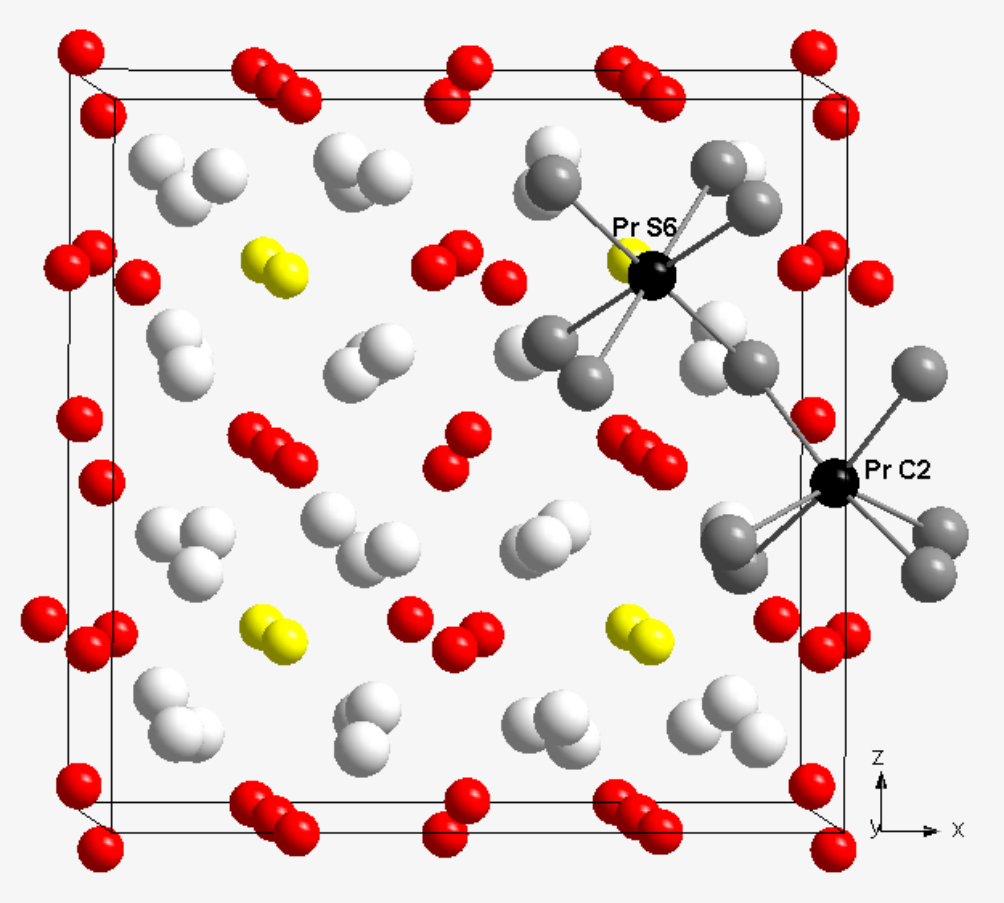

Figure 1. Pascual *et al.*

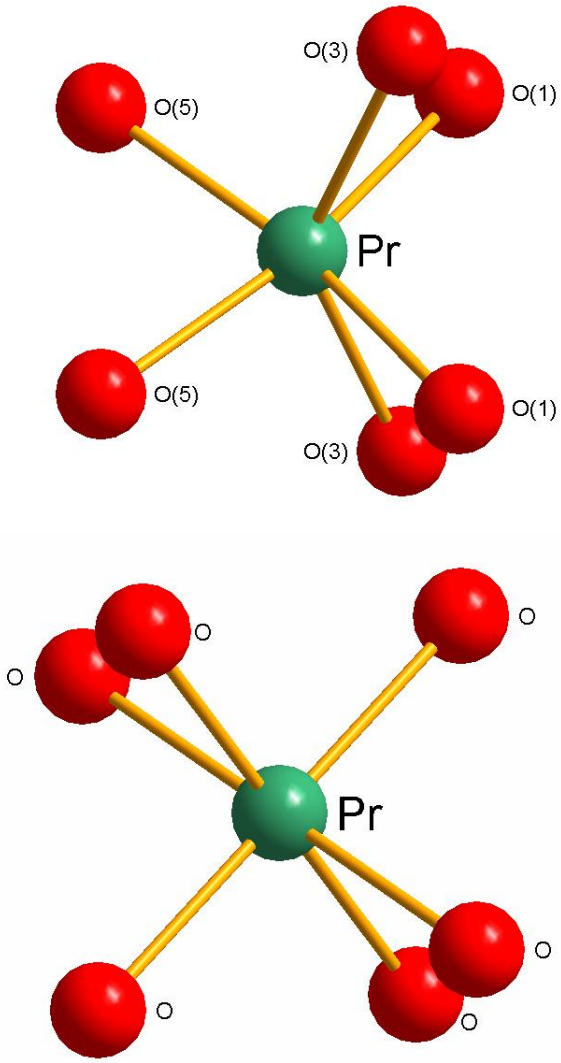

Figure 2. Pascual *et al.*

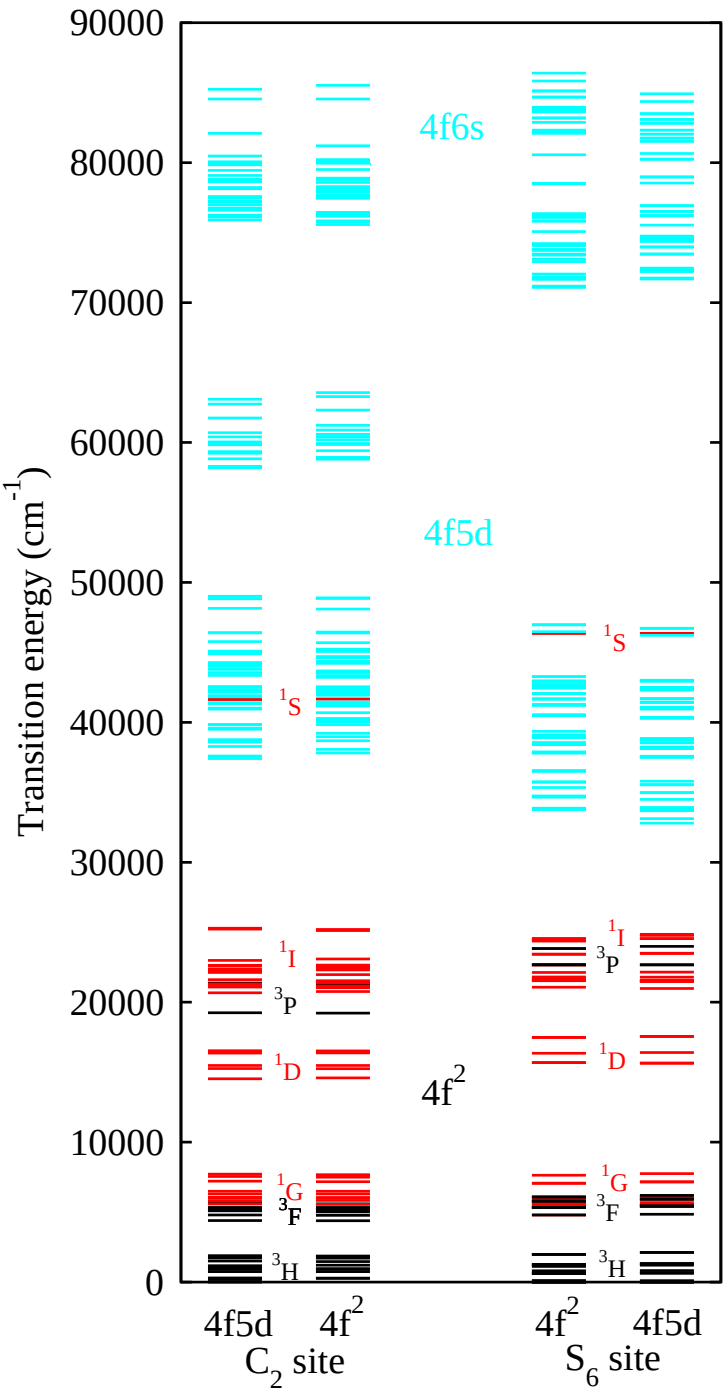

Figure 3. Pascual *et al.*